Exchange interactions in europium monochalcogenide magnetic semiconductors and their dependence on hydrostatic strain

W. Söllinger,[1] W. Heiss,[1] R. T. Lechner,[1] K. Rumpf,[2] P. Granitzer,[2] H. Krenn,[2] and G. Springholz[1,*]
[1]*Institute of Semiconductor and Solid State Physics, Johannes Kepler University, Altenbergerstrasse 69, A-4040 Linz, Austria*
[2]*Institute of Physics, Experimental Physics Div., Karl-Franzens-University, Universitätsplatz 5, A-8010 Graz, Austria*
(Received 27 July 2009; revised manuscript received 15 March 2010; published 23 April 2010)

The classical Heisenberg model is applied in a Monte Carlo study to investigate the distance dependence of the indirect nearest-neighbor (NN) exchange and next-nearest-neighbor (NNN) superexchange interaction in EuO, EuS, EuSe, and EuTe. For this purpose, first, the dependence of the magnetic ordering temperature, i.e., Curie, respectively, Néel temperature for ferromagnetic and antiferromagnetic ordering on the exchange constants was determined. This was then employed for the analysis of experimental data of hydrostatic pressure experiments. It is shown that all experimental findings, i.e., the strong increase in the critical temperatures as well as the transition from antiferromagnetic to ferromagnetic ordering for EuTe and EuSe with decreasing lattice parameter are well described by the magnetic Grüneisen law in which the exchange constants depend on the interatomic distances of the Eu ions in the form of a power law. According to these calculations, the indirect NN exchange is characterized by a Grüneisen exponent of approximately 20 and the NNN superexchange by an exponent of about 10 for all four europium monochalcogenides. The latter agrees with Bloch's empirical 10/3 law for the volume dependence of superexchange interactions in insulating magnetic materials. The Monte Carlo calculations also yield significantly revised exchange constants for unstrained bulk material because spin fluctuations at nonzero temperatures are taken into account. The strong increase in the exchange constants with decreasing lattice parameter provides room for increasing the Curie temperatures in strained epitaxial structures, which is important for device applications.

DOI: 10.1103/PhysRevB.81.155213 PACS number(s): 75.50.Pp, 75.10.Hk, 75.30.Et, 75.40.Mg

I. INTRODUCTION

The europium monochalcogenides (EuX, with X=O, S, Se, or Te) are wide band-gap magnetic semiconductors with cubic rock salt crystal structure and increasing lattice constant as X changes from O to Te.[1–3] They are considered to be model substances for Heisenberg magnets with spin ordering dominated by indirect nearest-neighbor (NN) exchange J_1 and next-nearest-neighbor (NNN) superexchange J_2 acting between the $S=7/2$ localized magnetic moments of the Eu^{2+} ions with half-filled $4f$ shells.[4] Depending on the sign and magnitude of the exchange integrals J_1 and J_2, the EuX's exhibit different magnetic phases below the critical ordering temperature.[5] EuO (Ref. 6) and EuS (Ref. 7) are ferromagnets (FMs) and EuTe (Ref. 8) is an antiferromagnet (AFM). EuSe is at the borderline between ferromagnetic and antiferromagnetic ordering. Thus, it shows metamagnetic behavior,[9–11] which is influenced by additional contributions from dipolar interactions and crystalline field anisotropies.

The EuX's show several outstanding properties, which makes them an interesting class of materials, both academically and for device applications. In external magnetic fields they exhibit a giant spin splitting of the conduction band and, consequently, extraordinary large magneto-optical effects. EuSe shows the largest effective g factor[12] of up to 18 000 and EuTe the largest magnetic field induced energy shifts of the interband transitions[13] observed in semiconducting materials. Potential applications are spin-filter devices based on EuO,[14–16] EuS,[17–24] or EuSe (Ref. 25) tunnel junctions, which provide spin-polarized electrons due to different barrier heights for electrons in different spin states. Also, a huge Faraday rotation is observed in EuX's (Refs. 26–29) due to the spin splitting of the bands, which results in different refractive indices for left and right circular polarized light. Therefore, EuS/EuF_2 and EuSe films have been used for high-resolution magneto-optical imaging of the flux distribution in superconductors.[30] Recent work has also demonstrated that EuO can be epitaxially grown on silicon[31,32] and GaN,[32] which opens new possibilities for device realization. Since the Curie temperature of the EuX's can be drastically enhanced by doping,[32–34] EuO might even become a candidate for practical spintronic device applications.

Introducing strain, either omniaxially through hydrostatic pressure[35–48] or biaxially through heteroepitaxial growth[11,49–53] leads to drastic changes in the ordering temperatures in the EuX compounds and in some cases even to transitions to different kinds of magnetic ordering. For EuO, hydrostatic pressure was found to increase the ferromagnetic ordering temperature T_C from 69 to above 200 K (Ref. 45) and for EuS from 16 to almost 180 K.[48] Metamagnetic EuSe is transformed to a stable ferromagnet already at moderate hydrostatic pressures above 0.5 GPa (Ref. 40) and at higher pressures T_C increases from 4.7 to 70 K at 15 GPa.[48] EuTe remains antiferromagnetic up to 9 GPa with nearly constant Néel temperature $T_N \approx 10$ K but then becomes ferromagnetic with a T_C increasing up to 28 K when reaching 17 GPa.[46]

The variations in the magnetic properties of the EuX compounds are obviously related to the dependence of the exchange integrals J_1 and J_2 on the interatomic distances in the crystal lattice. Already by early theoretical work, the basic trend of the EuX compounds from antiferromagnetic (EuTe) to ferromagnetic ordering (EuS and EuO) was attributed to a strong increase in the ferromagnetic NN exchange J_1 with

decreasing lattice constant from a_0=6.598 Å for EuTe to 5.144 Å for EuO. For the latter, the magnetic ordering is thus dominated by the positive NN exchange J_1, whereas for antiferromagnetic EuTe the negative NNN exchange J_2 dominates. Application of hydrostatic pressures p up to 20 GPa produces similar changes in the lattice parameter of up to 8% compared to the normal bulk values. As a result, large changes in the ordering temperatures are induced as well.[35–48]

To derive the dependence of the exchange integrals J_1 and J_2 on the interatomic distances from hydrostatic pressure experiments, previous works have employed the mean-field approximation (MFA) for analysis.[46,48,54] Based on the observation that the Néel temperature T_N of antiferromagnetic EuTe does not change appreciably under applied pressure, it was reasoned that the NNN exchange J_2 is constant in all EuX compounds. Therefore, the changes in the magnetic properties were attributed solely to changes in the NN exchange J_1 and, from the simple mean-field expressions, a distance dependence of $J_1(a)$ was deduced from the observed changes in $T_C(p)$. However, it is well known that the mean-field approximation is exact only at zero temperature, i.e., for prediction of the ground state of the system. In particular, the mean-field model vastly overestimates the magnetic ordering temperatures due to neglection of spin fluctuations at finite temperatures. As a result, the mean-field approximation not only predicts false critical exponents at the phase transition but also much underrated exchange constants.

In the present work, we have employed the Monte Carlo (MC) method to calculate the magnetic phase diagrams and ordering temperatures of the EuX compounds as a function of the exchange interactions. The MC method takes the mutual interactions between all spins into account and allows for spin fluctuations at T above zero. Using finite-size scaling techniques, MC correctly predicts the transition temperatures and the behavior of the order parameters at criticality for a given model Hamiltonian.[55] Moreover, due to the spin fluctuations near the transition temperature, the Néel point of antiferromagnetic ordering has been found to depend on both exchange constants[56] J_1 and J_2—in contrast to the mean-field approximation, where the Néel point depends on J_2 only. Thus, the basic assumption of the previous analyses[46,48,54] does not hold. In the present work, we therefore reexamine the experimental data for EuX's under hydrostatic pressure by Monte Carlo calculations considering magnetic Grüneisen power laws[57] for the distance dependence of the NN and NNN exchange constants. We show that for the whole family of EuX compounds, the distance dependence of the exchange interactions $J_1(r_1)$ and $J_2(r_2)$ can be consistently described by unique Grüneisen exponents of $n_1 \approx 20$ and $n_2 \approx 10$ by which the whole set of available experimental data of the EuX compounds under hydrostatic pressure can well be explained. The obtained exponent of $n_2 \approx 10$ for J_2 is also consistent with Bloch's empirical 10/3 law[57] for the volume dependence of the superexchange interaction $J \sim V^{-10/3}$ observed for a wide variety of insulating magnetic material systems.[57]

The paper is organized as follows: In Sec. II, we present the model Hamiltonian and briefly discuss the technical details of the Monte Carlo calculations. In Sec. III, the method is applied to bulk EuTe under ambient pressure, demonstrating that the whole magnetic phase diagram can be well described and that the exchange constants J_1 and J_2 obtained from Monte Carlo calculations strongly differ from literature values derived by the mean-field approximation. In Sec. IV, the method for determination of the distance dependence of the exchange constants is described and applied to EuTe. Due to the pressure-induced transition between antiferromagnetic and ferromagnetic ordering, accurate dependencies for both $J_1(r_1)$ and $J_2(r_2)$ are derived. The approach is then extended to EuO, EuS, and EuSe in Secs. V and VI, revealing that the same functional behavior, i.e., the same Grüneisen exponents provide an excellent description of the experimental data for all EuX compounds. In Sec. VII, the results are compared in detail and the applicability of other types of functional dependence of $J_1(r_1)$ and $J_2(r_2)$ discussed.

II. DETAILS OF THE CALCULATION

For the calculation of the magnetic properties of the EuX's we employed the classical Heisenberg model with nearest and next-nearest-neighbor exchange interactions taken into account. The corresponding model Hamiltonian reads as

$$\mathcal{H} = -\sum_{i \neq j} J_{ij} \boldsymbol{S}_i \boldsymbol{S}_j - g\mu_B \boldsymbol{H} \sum_i \boldsymbol{S}_i, \tag{1}$$

where $\boldsymbol{H}$ denotes the external magnetic field and $J_{ij}+J_{ji}$ is the total exchange interaction between two spins located at lattice sites i and j, where

$$J_{ij} = \begin{cases} J_1: & i \text{ is NN of } j \\ J_2: & i \text{ is NNN of } j \\ 0: & \text{else.} \end{cases} \tag{2}$$

In the Monte Carlo calculations, we consider rhombohedral fcc clusters of classical spins, where all cluster boundaries are (111) lattice planes. This is a convenient choice of geometry since antiferromagnetic and ferrimagnetic (FiM) ordering in EuSe and EuTe is comprised of ferromagnetic (111) planes and epitaxial EuTe and EuSe samples are usually grown in (111) orientation.[11–13,58] The choice of geometry has, however, no influence on the results of our calculations. Clusters of up to 32^3 spins with periodic boundary conditions were employed. During a single Monte Carlo step, random orientations are generated for every single spin, which are then accepted or rejected according to the Metropolis criterion.[59] Observables like the total energy, the overall magnetization, the magnetization in the direction of the external field, the transverse magnetization, and the corresponding staggered magnetic moments are computed after every Monte Carlo step. Simulations were performed with up to $N=10^5$ iterations and additional Monte Carlo steps for equilibration at the beginning of every run. For a single simulation, the temperature T, the external magnetic field H and the number of spins are constant.

The expectation value for the total energy is given by

$$\langle \mathcal{H} \rangle \approx \frac{\sum_{i=1}^{N} \mathcal{H}_i \exp(-\beta \mathcal{H}_i)}{\sum_{i=1}^{N} \exp(-\beta \mathcal{H}_i)}, \tag{3}$$

where $\beta = 1/k_B T$. The Metropolis algorithm causes the total energy to be distributed according to Boltzmann's law. Hence, the expectation values for the total energy and for the magnetic moment become arithmetic mean values in the simulation

$$\langle \mathcal{H} \rangle = \frac{1}{N} \sum_{i=1}^{N} \mathcal{H}_i, \tag{4}$$

$$\langle \boldsymbol{M} \rangle = \frac{1}{N} \sum_{i=1}^{N} \boldsymbol{M}_i. \tag{5}$$

To determine the critical ordering temperatures, the fourth-order cumulant of the corresponding order parameter is used, which for ferromagnetic ordering at zero external field is defined as[55]

$$U = 1 - \frac{\langle M^4 \rangle}{3 \langle M^2 \rangle^2}, \tag{6}$$

where $\langle M^2 \rangle$ and $\langle M^4 \rangle$ denote the second- and fourth-order moments of the probability distribution of the magnetization. The fourth-order cumulants show universal values at the critical temperature. Thus, during the simulations U is generated as a function of temperature and recorded for various cluster sizes. The $U(T)$ curves for different cluster sizes cross in a single point at the critical temperature, as shown in detail in Sec. III. The transition temperatures obtained from our calculations were compared to theoretical predictions from high-temperature series expansions.[60] For classical spins on a fcc lattice and ferromagnetic nearest-neighbor exchange only, i.e., $J_1 > 0$ and $J_2 = 0$, we obtain a critical temperature T_C defined by $2J_1 S^2/(k_B T_C) = 0.3149 \pm 0.0008$ in 2×10^5 Monte Carlo steps. The prefactor of 2 stems from the fact that according to the definition of Eq. (1), the exchange interaction between pairs of spins is always added twice. Despite the simplicity of our approach compared to more sophisticated Monte Carlo routines,[61,62] this result is in excellent agreement with the theoretically predicted and generally accepted value of Ritchie and Fisher[60] of 0.3147 ± 0.0001 for this relation.

If the NNN exchange interaction is antiferromagnetic and $|J_2| > J_1$, the simulation generates a classical Néel state with eight ferromagnetically ordered sublattices as the ground state.[63] This is a consequence of the antiferromagnetic ordering degenerating into the four equivalent (111) directions[52] in the simulation. In this case, four pairs of antiferromagnetically aligned sublattices can rotate freely and the fourth-order cumulants are defined as[63]

$$U^{st} = \frac{5}{2} - \frac{3}{2} \frac{\langle (M^{st})^4 \rangle}{\langle (M^{st})^2 \rangle^2} \tag{7}$$

for zero field and

$$U_{\perp}^{st} = 2 - \frac{\langle (M_{\perp}^{st})^4 \rangle}{\langle (M_{\perp}^{st})^2 \rangle^2} \tag{8}$$

for nonzero external field. Here, M^{st} and $M_{\perp}^{st}$ denote the staggered (transverse) magnetization, with transverse referring to the component of the magnetization perpendicular to the external field,

$$M^{st} = \sum_{i=1}^{8} |\boldsymbol{M}^{(i)}|, \tag{9}$$

$$M_{\perp}^{st} = \sum_{i=1}^{8} |\boldsymbol{M}_{\perp}^{(i)}|. \tag{10}$$

Equations (9) and (10) are sums of the absolute values of the (transverse) magnetization over the eight possible sublattices. Due to additional anisotropies and/or dipolar couplings, this degenerate AFM state is not observed experimentally but only domains with completely ferromagnetically ordered Eu (111) planes, which is one possible case in our MC simulations. Here it should also be noted that in a quantum-mechanical treatment it has been shown[64] that a classical Néel state is not an eigenstate of the system. However, Anderson[65] showed that the upper limit of the error introduced by utilizing the classical Heisenberg model is $1/(ZS)$, where Z is the number of nearest neighbors. Since the Eu ions carry a relatively large spin of $S = 7/2$, the error in the ground-state energy is smaller than 2.4%. Thus, a classical treatment considering continuously rotating spin vectors is well justified.

III. EXCHANGE INTERACTIONS IN EuTe AT AMBIENT PRESSURE

In our Monte Carlo study of the exchange interactions, EuTe is chosen as test material. This is because detailed experimental data is available for the H-T phase diagram,[8] which allows a direct determination of the NN and NNN exchange interactions J_1 and J_2 based on the antiferromagnetic ordering temperature T_N and the critical field at zero temperature $H_C(T=0)$. In addition, the ferromagnetic (J_1) and the antiferromagnetic exchange (J_2) are relatively balanced in EuTe. Therefore, pronounced changes in magnetic ordering occur when hydrostatic pressure is applied.

A. Experimental results

The magnetic properties of EuTe were determined using dc and ac superconducting quantum interference device (SQUID) magnetometry measurements of high quality 4-μm-thick (111)-oriented epitaxial layers grown by molecular-beam epitaxy on BaF_2 substrates.[13,66,67] As a result, the magnetization and ac susceptibility was obtained as a function of both temperature and external magnetic field up

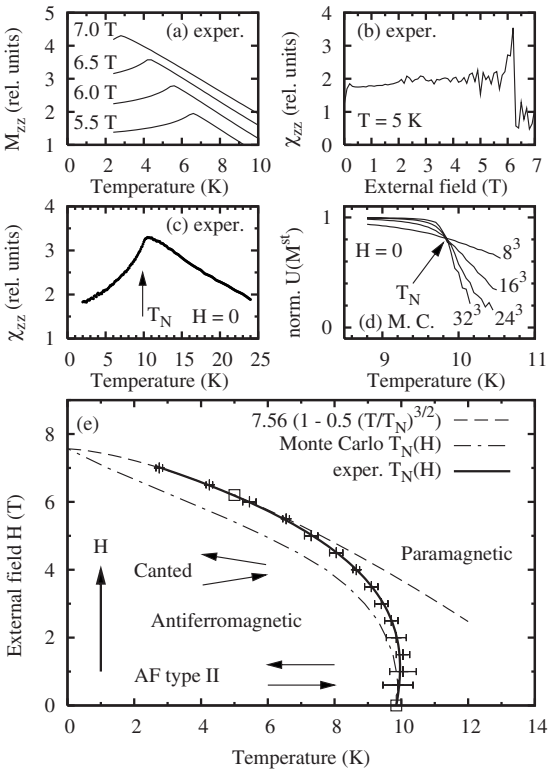

FIG. 1. Magnetic properties of bulk EuTe at normal pressure derived from SQUID and Monte Carlo simulations. (a) Measured temperature-dependent magnetization $M(T)$ for various in-plane external magnetic field values from 5.5 to 7 T. (b) ac susceptibility vs external magnetic field at 5 K, indicating the critical field as discontinuity at $B \approx 6.2$ T. (c) ac susceptibility χ measured as a function of temperature at zero external field. The inclination point indicated by the arrow yields a Néel temperature of 9.85 ± 0.05 K. (d) Determination of the Néel temperature from Monte Carlo data using the fourth-order cumulant of the staggered magnetization $U(M^{st})$ for different system sizes. The curves show a common intersection at the Néel temperature. (e) Magnetic phase diagram of EuTe: symbols with error bars correspond to maxima or inflection points in the experimental $M(T)$ for high, respectively, small external fields; squares to the discontinuity in $\chi(H)$ or the inflection point in $\chi(T)$. The solid line indicates the experimental $H_C(T)$ phase boundary and the dashed-dotted line represents the boundary obtained by the Monte Carlo calculations. The $T^{3/2}$ extrapolation (dashed line) of the experimental data toward $T=0$ yields a critical field of $H_C=7.56$ T.

to 7 T. The external field direction was applied in the (111) growth plane, which is also the easy plane of the magnetization.

Experimental magnetization curves $M(T)$ at different applied external fields from 5.5 to 7 T are shown in Fig. 1(a). The magnetization curves exhibit clear peaks at the phase transition between the antiferromagnetic and the paramagnetic phase. High magnetic fields were applied in order to obtain information about the critical field at zero temperature $H_C(T=0)$. Field-dependent ac susceptibility curves were also measured. As shown in Fig. 1(b), for $T=5$ K the susceptibility is essentially constant below the critical field, corresponding to a linear increase in the magnetization. This arises from the continuous reduction in the relative angle between the spins in the adjacent (111) lattice planes from 180° in the AFM II state at zero field to almost zero at the critical field H_C, as illustrated schematically by the arrows in Fig. 1(e). Thereby, the spin orientation changes from initially perpendicular to the external field to finally parallel to the external field direction when H reaches the critical field. The critical field is thus given by the discontinuous drop in the susceptibility at this point [see Fig. 1(b)].

Figure 1(c) displays the measured susceptibility as a function of temperature at zero external field, showing a broad peak with a maximum slightly above 10 K. However, the phase transition from antiferromagnetic to paramagnetic corresponds to the peak in the specific heat, which according to Fisher's rule[68] coincides with the maximum slope, i.e., the inclination point in the ac susceptibility. As indicated by the arrow in Fig. 1(c), the phase transition thus occurs at $T_N = 9.85 \pm 0.05$ K.

Figure 1(d) shows the phase diagram of EuTe compiled from the experimental data (symbols and solid line), where the thick solid line indicates the experimentally determined $H_C(T)$ phase boundary. A $T^{3/2}$ curve, which according to spin-wave theory is the low-temperature behavior of the critical field, was fitted to the experimental critical points between 2 and 6 K, yielding

$$H_C(T) = H_C(0)[1 - \lambda(T/T_N)^{3/2}]. \tag{11}$$

Extrapolation of the measured $H_C(T)$ to $T=0$ thus yields the critical field at zero temperature of $H_C(0)=7.56 \pm 0.02$ K. The dashed line in Fig. 1(e) represents Eq. (11) with the coefficient $\lambda = 0.50 \pm 0.01$. The experimental data as well as T_N, $H_C(0)$, and λ are in excellent agreement with previous results of Oliveira *et al.*[8]

B. Exchange constants and phase diagram from MC calculations

In most previous studies,[1,2,8,69] the mean-field analysis was used to determine the exchange integrals in EuTe because it provides simple analytic expressions for the critical field at zero temperature $H_C(0)$, the Néel temperature T_N, as well as the paramagnetic Curie temperature θ_C as a function of J_1 and J_2. For type II-antiferromagnetic ordering in an fcc lattice with NN and NNN exchange interactions, the MFA yields

$$H_C^{\mathrm{MFA}}(0) = -4S(6J_1 + 6J_2)/(g\mu_B), \tag{12}$$

$$T_N^{\mathrm{MFA}} = \frac{2}{3}S(S+1)(-6J_2)/k_B, \tag{13}$$

and

$$\theta_C^{\mathrm{MFA}} = \frac{2}{3}S(S+1)(12J_1 + 6J_2)/k_B, \tag{14}$$

where $g=2$ and $S=7/2$ for the magnetic moment of the Eu^{2+} ions. Inserting our experimental values for $H_C(0)$ and T_N into Eqs. (12) and (13) and solving for J_1 and J_2 yields for $J_1^{\mathrm{MFA}}/k_B = 0.035$ K and for $J_2^{\mathrm{MFA}}/k_B = -0.156$ K. As shown

TABLE I. Comparison of the exchange constants J_1/k_B and J_2/k_B of EuTe determined by the analysis of experimental data for the Néel temperature T_N, the critical field H_C, or the paramagnetic Curie temperature θ_C using the MFA (Refs. 1, 2, 8, and 69) or the MC method (present work). Also listed are the exchange constants derived by Kuneš *et al.* (Ref. 70) from *ab initio* calculations.

Reference	Measurement/analysis	J_1/k_B (K)	J_2/k_B (K)
Oliveira (Ref. 8)	H_C, θ/MFA	0.100	−0.215
Zinn (Ref. 1)	H_C, θ/MFA	0.060	−0.200
Wachter (Ref. 2)	H_C, T_N/MFA	0.043	−0.150
Köbler (Ref. 69)	H_C, T_N/MFA	0.060	−0.160
Kuneš (Ref. 70)	*Ab initio* LDA+U (U=6 eV)	0.110	−0.320
Our study	H_C, T_N/MFA	0.035	−0.156
	H_C, T_N/MC	0.192	−0.313

in Table I, the values are consistent with previous mean-field studies,[1,2,8,69] especially those, which applied the same analysis of the experimental $H_C(0)$ and T_N based on MFA Eqs. (12) and (13).

In the Monte Carlo calculations, the transition temperature $T_N(0)$ ($T_N(H\neq 0)$) is deduced from the temperature dependence of the fourth-order cumulants of the staggered (transverse) magnetization $U^{st}_{(\perp)}$. As described in Sec. II, these cumulants show universal values at the critical temperature T_N independent of cluster size. This is demonstrated in Fig. 1(d) for the case of H=0. Using the exchange constants J_1^{MFA} and J_2^{MFA} derived from the mean-field analysis, the Monte Carlo calculations yield a Néel temperature of 5.45 K at zero external field, which is in strong disagreement with the experimental value of 9.85 K. This clearly demonstrates that the neglection of spin fluctuations in MFA leads to a vast underestimation of the exchange constants, an effect that has been already noted in previous theoretical studies.[56,63] In the MC calculations, moreover, the critical Néel temperature T_N is found to depend significantly not only on the antiferromagnetic exchange constant J_2 but also on the ferromagnetic NN exchange constant J_1, in contrast to the MFA approximation, where T_N^{MFA} depends only on the antiferromagnetic exchange—see Eq. (13). This is due to the fact that in the mean-field approximation, for type II antiferromagnetic ordering the J_1 exchange between the six NN Eu^{2+} ions within the ferromagnetic (111) planes exactly cancels with the J_1 exchange to the six NN Eu^{2+} ions within the antiferromagnetically coupled neighboring (111) lattice planes. This does not apply for the MC calculations because of the nonperfect antiferromagnetic spin alignment at nonzero temperatures that results from spin fluctuations.

In order to determine the exchange constants from the Monte Carlo calculations, we have systematically calculated the Néel temperature as a function of both exchange constants J_1 and J_2. As a boundary condition, we take advantage of the fact that in the limit of T=0, the critical field H_C, the Monte Carlo calculations converges exactly to the mean-field value of Eq. (12). This is because spin fluctuations are absent at T=0 and thus the MFA represents the exact ground state of the system. Therefore, the experimental value of H_C =7.56 T at T=0 and Eq. (12) determine the sum of the exchange constants as

$$(J_1 + J_2)/k_B = -0.121 \ \mathrm{K} \tag{15}$$

in EuTe. This eliminates one independent variable, i.e., with this condition, only J_2 must be varied for the calculation of T_N. The resulting dependence is plotted in Fig. 2 (squares and solid line). Evidently, T_N varies almost perfectly linearly and can be represented by the relation

$$T_N^{\mathrm{MC}}|_{(J_1+J_2)/k_B=-0.121\ \mathrm{K}} = 1.22 - 27.57 J_2/k_B \tag{16}$$

within the range $-0.35\ \mathrm{K} \leq J_2/k_B \leq -0.15$ K. Solving Eq. (16) for J_2 and inserting the experimental Néel point of bulk EuTe T_N=9.85 K (horizontal dashed-dotted line in Fig. 2) yields J_2^{MC}/k_B=−0.313 K and hence J_1^{MC}/k_B=0.192 K from Eq. (15) as the intrinsic exchange constants of bulk EuTe. It is noted that calculating T_N without the constraint of Eq. (15) yields a function $T_N(J_1,J_2)$ that depends nonlinearly on J_1 and J_2, in contrast to the MFA Eq. (13), which predicts only a linear dependence on J_2—see Sec. IV for further details. From the MC calculations, the Néel temperature as a function of J_1 and J_2 is found to be well described by

$$T_N^{\mathrm{MC}} \approx (-15.3J_1 - 40.8J_2)/k_B$$
$$= \frac{2}{3}S(S+1)(-1.46J_1 - 3.89J_2)/k_B \tag{17}$$

in a linear approximation in the vicinity of the intrinsic EuTe exchange constants, demonstrating that the Néel temperature indeed depends strongly on both exchange constants.

As demonstrated by Table I, which compares our derived set of exchange constants with previously published ones, our values are nearly twice as large as those derived from mean-field analysis. Thus, by neglection of spin fluctuations the exchange parameters are vastly underestimated. Remarkably, the exchange constants derived from our Monte Carlo

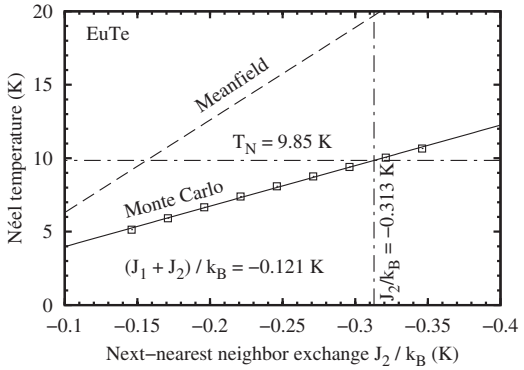

FIG. 2. Néel temperature of EuTe (squares) calculated as a function of the next-nearest-neighbor exchange constant J_2 under the constraint $(J_1+J_2)/k_B$=−0.121 K, which is a consequence of evaluating the experimental critical field at zero temperature $H_C(T=0)$—see in the text for details. A linear function is obtained by the Monte Carlo calculations (squares and solid line), which is shown in comparison with the corresponding mean-field relation (dashed line). At J_2/k_B=−0.313 K (J_1/k_B=0.192 K) the Monte Carlo curve reaches the experimental Néel point of 9.85 K.

calculations are in good agreement with recent *ab initio* calculations of Kuneš *et al.*[70] using the local-density-approximation method including strong Coulomb repulsion within the $4f$ shells (LDA+U). In particular, our NNN exchange constant J_2, which in Ref. 70 of Kuneš *et al.* depends very weakly on the Coulomb parameter U matches the *ab initio* result very well.

With the new exchange parameters, we can now calculate the whole magnetic phase diagram of EuTe using the fourth-order cumulants of the staggered (transverse) magnetization for various external magnetic fields and cluster sizes. The resulting phase boundary $T_N(H)$ is depicted as dashed-dotted line in Fig. 1(e). As expected, the calculated $H_C(T)$ approaches the experimental value of 7.56 T in the limit of $T \rightarrow 0$ and nearly follows the experimental $H_C(T)$ boundary. The fact that at $T>0$ the calculated $H_C(T)$ values are slightly lower than the measured ones and that at low temperatures, the calculated critical field varies linearly with temperature instead of obeying a $T^{3/2}$ behavior is a well-known consequence of applying a classical ($S=\infty$) instead of the quantum-mechanical $S=7/2$ model in our calculations. As already noted in Sec. II, the error in the ground-state energy introduced by this simplification is on the order of less than 2.4% for our type of system.

IV. DISTANCE DEPENDENCE OF EXCHANGE INTERACTIONS IN EuTe

Using hydrostatic pressure, the EuTe lattice constant can be compressed from its normal bulk value of $a_0=6.589$ Å to about 6.15 Å at a pressure reaching 17 GPa.[46] This corresponds to a 7% reduction in the lattice constant and of the interatomic distances of the Eu^{2+} ions in the crystal, where in the fcc lattice of EuTe the NN Eu^{2+} distance $r_1=a/\sqrt{2}$ and the NNN distance $r_2=a$. The resulting changes in the magnetic ordering temperatures obtained by such experiments[38,46,47] are compiled in Fig. 3, where the open and full symbols represent the measured T_N, respectively, T_C values plotted as a function of EuTe lattice constant. Since at ambient pressure, the antiferromagnetic exchange J_2 of EuTe is larger than the ferromagnetic exchange J_1, a type II antiferromagnetic ordering[5] occurs below the Néel point of $T_N=9.85$ K. As shown in Fig. 3, with increasing pressure, i.e., decreasing lattice constant, the Néel temperature remains practically constant at $T_N \approx 10$ K but at ≈ 9 GPa or 5% compressive strain EuTe becomes ferromagnetic[46,47] with rapidly increasing Curie temperature T_C that rises up to 28 K at 17 GPa.[46] The observed phase transition from antiferromagnetism to ferromagnetism at $a=6.29$ Å implies that at smaller atom distances, the NN exchange J_1 becomes the dominating exchange mechanism.

The influence of the interatomic distances r_i on exchange constants has been a subject of many theoretical studies.[1,4,54,71–73] However, indirect and superexchange mechanisms involve complex integrals such that up to now no general analytic expressions for their distance dependence have been derived theoretically. An empirical power-law dependence, referred to as the magnetic Grüneisen law, has been proposed by Bloch,[57] i.e.,

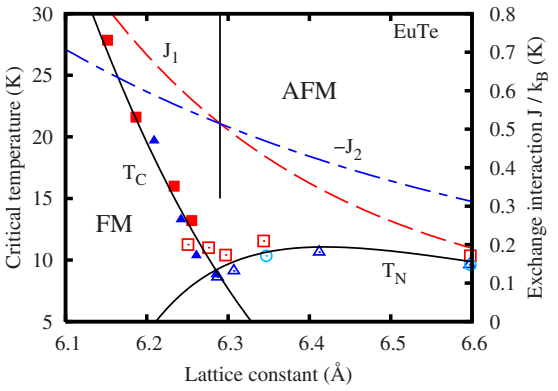

FIG. 3. (Color online) Critical temperatures (left scale) and exchange interactions J_1 and J_2 (right scale) in EuTe plotted as a function of the lattice constant a. Open and closed symbols [circles (Ref. 38), squares (Ref. 46), and triangles (Ref. 47)], correspond to measured Néel (T_N), respectively, Curie points (T_C) determined from hydrostatic pressure experiments. Solid lines: $T_N(a)$ and $T_C(a)$ derived from Monte Carlo calculations using a $J_1(a)$ and $J_2(a)$ dependence given by the Grüneisen law [Eq. (18)] with best fitting power-law exponents of $n_1=20.6\pm0.4$ and $n_2=10.4\pm0.5$, respectively. The corresponding dependence of $J_1(a)$ and $J_2(a)$ as a function of the lattice parameter is shown as the dashed and dashed-dotted line, respectively.

$$J(r) = J_0\left(\frac{r}{r_0}\right)^{-n}, \tag{18}$$

where $J_0=J(r_0)$ and r_0 are the exchange interaction and interatomic distance at normal pressure and n is the scaling exponent. As shown in Ref. 57, this dependence well describes the observations for many magnetic semiconductors or insulators such as the Mn and Gd chalcogenides or iron oxides, for which the power-law exponent n shows a universal value of around 10 for the magnetic superexchange.[57] This also yields the empirical 10/3 law for the volume dependence of superexchange[57] of $J(V)=J_0(V/V_0)^{-10/3}$.

To test if the Grüneisen dependence of Eq. (18) adequately describes the atomic distance dependence of the exchange integrals in EuTe, we have performed a series of Monte Carlo calculations of the Néel and Curie temperature as a function of the exchange integrals in order to fit the experimental $T_N(a)$ and $T_C(a)$ data of Fig. 3 using independent power-law exponents n_1 and n_2 for the NN and NNN exchange interactions J_1 and J_2 as free parameters. In these calculations, the ferromagnetic NN exchange $J_1(>0)$ and the antiferromagnetic NNN exchange $J_2(<0)$ were varied independently in the range of $0.190 \leq J_1/k_B \leq 0.73$ and $0.315\ \text{K} \leq -J_2/k_B \leq 0.615$ K and the corresponding critical temperatures were derived as described in detail in Secs. II and III. For all $|J_1|<|J_2|$, the MC calculations yield AFM II ordering, whereas FM ordering results for all $|J_1|>|J_2|$. Figures 4(a) and 4(b) show the calculated T_N and T_C values (open symbols) as a function of J_1 and J_2, respectively. Since we are interested in the hydrostatic pressure effect, the smallest values of J_1 and J_2 were chosen close to the exchange parameters of bulk EuTe at ambient pressure (filled symbols)

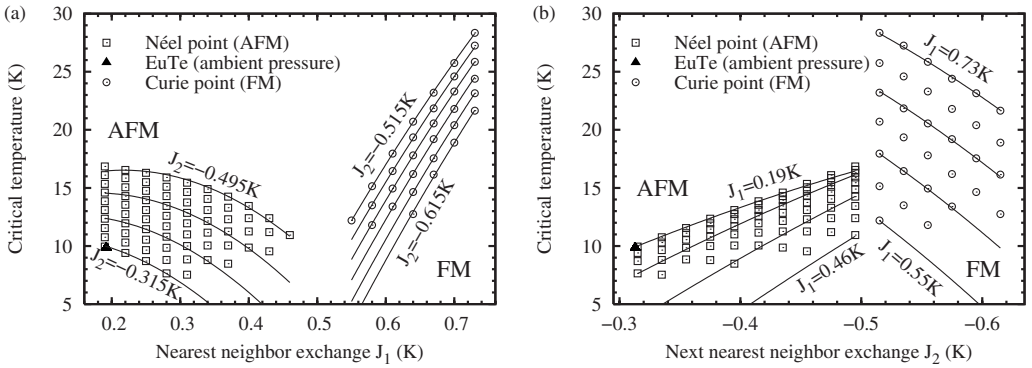

FIG. 4. Monte Carlo calculated critical temperatures of a bulk fcc Heisenberg system as a function of the strength of (a) the nearest-neighbor exchange interaction J_1 and (b) the next-nearest-neighbor exchange interaction J_2, showing antiferromagnetic to paramagnetic transitions (squares) when $J_1 < |J_2|$ and ferromagnetic to paramagnetic transitions (circles) when $J_1 > |J_2|$. The solid lines represent polynomial fit functions, which are quadratic in J_1 and J_2.

and the maximum values correspond to hydrostatic pressures of about 17 GPa.

As shown by Fig. 4, the Monte Carlo calculations yield a strongly nonlinear dependence of T_N on J_1. Hence, the calculated data points were approximated by second degree polynomials for $T_N(J_1,J_2)$ and $T_C(J_1,J_2)$ of the general form

$$T(J_1,J_2) = A + BJ_1 + CJ_2 + DJ_1^2 + EJ_1J_2 + FJ_2^2. \quad (19)$$

These approximations fit the Monte Carlo data with better than ± 0.1 K accuracy and are represented as solid lines in Figs. 4(a) and 4(b).

Using the normal pressure exchange constants $J_{1,0} = 0.192$ K and $J_{2,0} = -0.313$ K determined in Sec. III, the two branches of hydrostatic pressure data sets for the antiferromagnetic $T_N(a)$ and ferromagnetic $T_C(a)$ of Fig. 3 were fitted using Eqs. (18) and (19) with common exponents n_1 and n_2 and $r_1 = a/\sqrt{2}$ and $r_2 = a$. All experimental data points are weighted equally in the least-square fit routine, which was performed on a logarithmic scale since equal weights may cause one branch to dominate if there is a difference in the magnitude of the dependent variable.

From this modeling, a Grüneisen exponent of $n_1 = 20.6 \pm 0.4$ for the NN exchange J_1 and of $n_2 = 10.4 \pm 0.5$ for the NNN exchange J_2 was obtained. As demonstrated by the solid lines in Fig. 3, with these parameters the whole body of experimental findings, i.e., the approximately constant Néel temperature T_N at small hydrostatic strain, the transition from antiferromagnetic to ferromagnetic ordering at $a = 6.29$ Å and the steep superlinear increase in the Curie temperature at small lattice constants and high hydrostatic pressures, are exactly reproduced. Moreover, the obtained power-law exponent n_2 for $J_2(r_2)$ is in excellent agreement with Bloch's (Ref. 57) 10/3 law for the volume dependence of superexchange.

Such obtained dependence of the NN and NNN exchange integrals $J_1(a)$ and $J_2(a)$ as a function of lattice parameter a is presented in Fig. 3 as dashed and dashed-dotted line, respectively. Evidently, both exchange constants strongly increase with decreasing lattice constant. However, $J_1(a)$ increases much more rapidly than $J_2(a)$ due to the two times larger power-law exponent. Therefore, the two curves intersect at $a = 6.29$ Å, where $J_1/k_B = -J_2/k_B = 0.51$ K, and at smaller a, the ferromagnetic J_1 becomes the dominating exchange mechanism. For fcc lattices with competing ferromagnetic NN exchange and antiferromagnetic NNN exchange interactions, this is exactly the condition for the material to become ferromagnetic.[5]

Our results are in severe contrast to the previous mean-field analysis of Goncharenko and Mirebeau,[46] who concluded from the negligible variation in T_N in the antiferromagnetic state with changing lattice constant that the NNN exchange J_2 in EuX should *not* depend on the lattice parameter. Consequently, the whole variation in $T_C(a)$ was attributed solely to changes in $J_1(a)$ using the mean-field expression for the Curie temperature of

$$T_C^{\mathrm{MFA}} = \frac{2}{3}S(S+1)(12J_1 + 6J_2)/k_B \quad (20)$$

with constant J_2 for data analysis. On the contrary, our calculations show that the broad plateau of $T_N(a)$ for lattice constants around $a = 6.42$ Å just results from the fact that in the antiferromagnetic phase the ferromagnetic exchange drops faster than the antiferromagnetic exchange as the lattice constant increases.

V. EXCHANGE INTERACTIONS IN EuO AND EuS

As shown in the previous sections, the exchange constants obtained by Monte Carlo calculations strongly differ from previously published values. Therefore, to evaluate the distance dependence of the exchange constants of EuO and EuS, first the bulk values under ambient pressure have to be re-examined by the Monte Carlo method.

A. Exchange constants at ambient pressure

EuO and EuS are low-temperature ferromagnets with Curie temperatures T_C of 69.15 K (Ref. 74) and 16.6 K,[74,75] respectively. The magnetic properties are determined mainly by the dominant ferromagnetic NN exchange interaction J_1 in both materials. Compared to the case of antiferromagnetic EuTe, where only the Néel temperature and the critical field

at $T=0$ K are needed to deduce the exchange constants, the determination of J_1 and J_2 for ferromagnetic EuO and EuS is much more involved. As a result, there exists a substantial variation in the reported exchange constants for bulk EuO and EuS deduced from different experimental techniques such as inelastic neutron scattering,[74–76] specific heat,[77–80] nuclear magnetic resonance[80–83] (NMR), and spin-wave resonance measurements[84] (see, e.g., Passell *et al.*[74] for a review). Especially the values for the NNN exchange constant J_2 in EuO and EuS differ by up to a factor of 2 in literature[74,76,83] and whether J_2 is ferromagnetic or antiferromagnetic in EuO is still a matter of debate. The most recent results based on inelastic neutron-scattering studies on single crystals of EuO (Ref. 76) and EuS (Ref. 75) yielded $(J_{1,0}^{\mathrm{EuO}}/k_B, J_{2,0}^{\mathrm{EuO}}/k_B)=(0.625\ \mathrm{K}, 0.125\ \mathrm{K})$ and $(J_{1,0}^{\mathrm{EuS}}/k_B, J_{2,0}^{\mathrm{EuS}}/k_B)=(0.221\ \mathrm{K}, -0.100\ \mathrm{K})$, respectively, consistent with Passell *et al.*'s (Ref. 74) analysis on powdered samples. Notably, a ferromagnetic NNN exchange interaction was obtained for EuO.

In all studies, the sum of $J=J_1+J_2$ has been more reliably determined than the individual NN and NNN exchange interactions, and this sum is quite consistent among the various studies. For EuO single crystals, $J^{\mathrm{EuO}}/k_B=0.755$ K was obtained by Comment *et al.*[83] from NMR measurements, in agreement with neutron-scattering studies by Mook *et al.*,[76] and this value also agrees with the results obtained by neutron-scattering[74] and specific-heat measurements[80] on powdered samples. A very good agreement for J_1+J_2 also exist among respective studies for EuS,[74,75,80,81] from which we calculate $J^{\mathrm{EuS}}/k_B=0.121\pm0.003$ K as mean value.

To determine the exchange constants by the Monte Carlo method, we again performed a series of calculations for the model Heisenberg Hamiltonian of Eq. (1) with the NN and NNN exchange interactions J_1 and J_2 varied independently over a wide range of $0.5\ \mathrm{K}\leq J_1/k_B\leq 2.5$ K and $-0.8\ \mathrm{K}\leq J_2/k_B\leq +0.4$ K. We find ferromagnetic ordering for all combinations of $J_1>-J_2$ and the corresponding critical ordering temperature determined as a function of J_1 and J_2 are depicted in Figs. 5(a) and 5(b), respectively. Evidently, T_C increases linearly with increasing NN exchange constant J_1, but *decreases* when the antiferromagnetic J_2 exchange increases. As shown by the solid lines in Fig. 5, in the range of studied exchange constants the dependence of T_C on the exchange constants can be well described by the relation

$$T_C^{\mathrm{MC}} = 79.0J_1/k_B + 55.9J_2/k_B$$
$$= 0.627\frac{2}{3}S(S+1)12(J_1+0.708J_2)/k_B, \qquad (21)$$

which differs considerably compared to the mean-field expression of Eq. (20). Yet, the critical coupling $J_1/(k_BT_C)$ closely resembles the theoretical predictions from high-temperature series expansion.[60] Inserting the EuO and EuS exchange values of Mook[76] and Bohn *et al.*[75] in our Monte Carlo relation of Eq. (21) yields Curie temperatures of only 56 and 12 K, respectively, which is much lower than the measured experimental values. This shows that, like for EuTe, the exchange constants have been considerably underestimated in both materials.

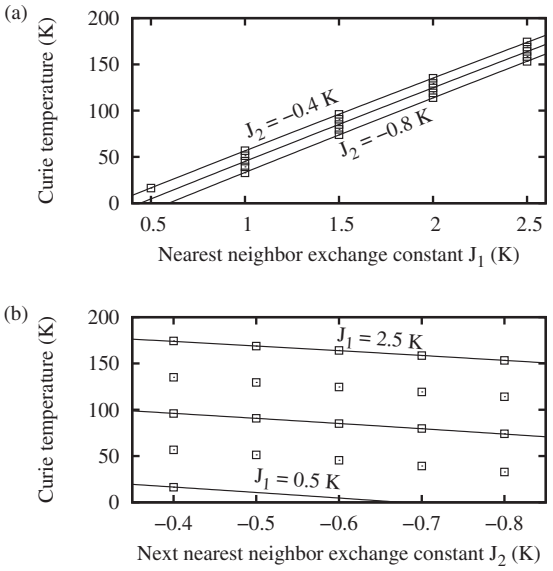

FIG. 5. Monte Carlo calculated critical temperatures of a bulk fcc Heisenberg system as a function of the strength of (a) the nearest and (b) next-nearest-neighbor exchange interactions J_1 and J_2, respectively, showing ferromagnetic to paramagnetic transitions if $J_1>-J_2$. The parameter range covers EuO and EuS under hydrostatic pressures between 0 and 20 GPa. Solid lines represent fit functions, which are linear in J_1 and J_2—see Eq. (21).

Using the experimental values for $J=J_1+J_2$ quoted above, the critical Curie temperature T_C can be calculated as a function of the exchange constant J_1 using Eq. (21) and $J_2=J-J_1$. The results are plotted as solid lines in Figs. 6(a) and 6(b) for EuO ($J^{\mathrm{EuO}}=0.755$ K) and EuS ($J^{\mathrm{EuS}}=0.121$ K), respectively. From the intersection of these lines with the respective experimental T_C values of 69.15 (Ref. 74) and 16.6 K (Refs. 74 and 75) (horizontal dashed lines in Fig. 6), the bulk exchange constants of $J_1^{\mathrm{EuO}}=1.169$ K and $J_2^{\mathrm{EuO}}/k_B=-0.414$ K are obtained for EuO and of $J_1^{\mathrm{EuS}}/k_B=0.427$ K and $J_2^{\mathrm{EuS}}/k_B=-0.306$ K for EuS. In Fig. 6, also plotted are the T_C values expected from the mean-field approximation [dashed-dotted line, Eq. (20)] as well as from a series expansion estimate proposed by Passell *et al.*[74] (dashed line) given by

$$T_C^{\mathrm{SE,est.}} = 0.790\frac{2}{3}S(S+1)12(J_1+0.619J_2)/k_B. \qquad (22)$$

Evidently, in both cases, much higher critical temperatures are predicted for a given set of exchange constants, i.e., from the observed transition temperatures, the exchange integrals are strongly underestimated. Moreover, a ferromagnetic NNN exchange would be suggested for EuO. Our Monte Carlo calculations rule out such a ferromagnetic NNN exchange under the condition that $J^{\mathrm{EuO}}/k_B=0.755$ K. In particular, a negative J_2 is retained even if J^{EuO} is increased by as much as 15%. Thus, as already found for the EuTe case, our Monte Carlo calculations greatly revise the bulk exchange constants.

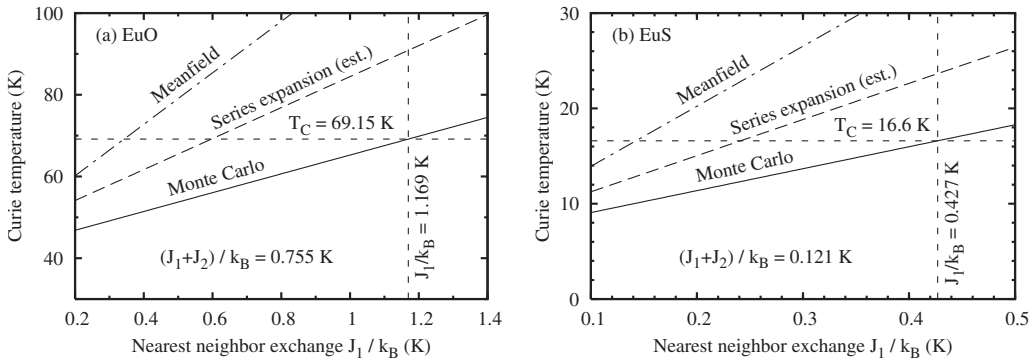

FIG. 6. Determination of the nearest-neighbor exchange constant $J_{1,0}$ of bulk (a) EuO and (b) EuS from Monte Carlo calculations (solid lines) under the constraint of constant $J=J_1+J_2=0.755$ K and 0.121 K for EuO and EuS, respectively, taken from experiments of Refs. 83 and 75. The dependence of the Curie temperature on J_1 predicted by mean-field approximation (dashed-dotted line) and series expansion (Ref. 74) (dashed line) is shown for comparison. The dashed horizontal lines indicate the experimental T_C values of 69.15 and 16.6 K for bulk EuO and EuS, respectively.

B. Distance dependence of EuO and EuS exchange constants

Under hydrostatic pressure, the Curie temperature T_C of EuO and EuS strongly increases with decreasing lattice constant. This is illustrated by Figs. 7 and 8, where the experimentally determined T_C values of EuO (Refs. 35, 44, and 45) and EuS (Ref. 48) are plotted as a function of the lattice constant. At hydrostatic pressures around 20 GPa, corresponding to a 6–8 % reduction in the lattice constant, T_C is as high as 200 (Ref. 45) and 180 K (Ref. 48) for EuO and EuS, respectively. For EuO, the experimental data $T_C(a)$ of Fig. 7 is compiled from three independent investigations,[35,44,45] with McWhan *et al.*'s data combined with the pressure-volume relation taken from Ref. 85. For EuS, the data are taken from Ref. 48. For EuO, experiments at even higher hydrostatic pressures up to 31 GPa (Ref. 45) have revealed that the ferromagnetic ground state becomes unstable at around 23 GPa and that the Curie temperature drops sharply afterward instead of further increasing. In Ref. 45 this behavior was attributed to *sf* hybridization competing with *sf* exchange in this pressure range, whereas in Ref. 86 an $Eu^{2+} \rightarrow Eu^{3+}$ valence transition and insulator to metal transition was proposed to occur. Therefore, we restrict our analysis to the 0–20 GPa range, i.e., lattice constants above 4.9 Å, where such effects seem not to be of importance.

To determine the interatomic distance dependence of the exchange constants, we proceed in the same manner as described in Sec. IV by fitting the calculated $T_C^{\mathrm{MC}}(J_1,J_2)$ dependence of Eq. (21) obtained by the Monte Carlo calculations to the data of the hydrostatic pressure experiments, applying the magnetic Grüneisen law [Eq. (18)] as functional dependence for the NN and NNN exchange constants. As input parameters we use the bulk exchange constants $J_{1,0}^{\mathrm{MC}}$ and $J_{2,0}^{\mathrm{MC}}$ determined in the previous section and treat the power-law exponents n_1 and n_2 in Eq. (18) as adjustable parameters. It

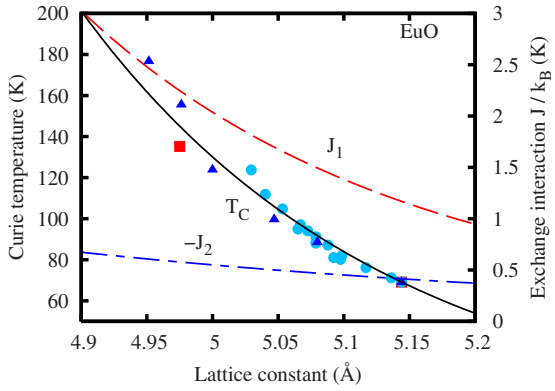

FIG. 7. (Color online) Critical Curie temperature and exchange interactions J_1 and J_2 in EuO plotted as a function of lattice parameter. Filled symbols [circles (Ref. 35), triangles (Ref. 44), and squares (Ref. 45)] correspond to measured Curie points in hydrostatic pressure experiments; the solid line represents the least-square fit of Monte Carlo critical temperatures $T_C(J_1,J_2)$ based on the magnetic Grüneisen law $J_i(r_i) \sim r_i^{-n_i}$ and $n_1=19.6$ and $n_2=10$. The corresponding dependence of the nearest (J_1) and next-nearest-neighbor exchange interaction (J_2) on the lattice parameter is presented by the dashed and dashed-dotted line, respectively.

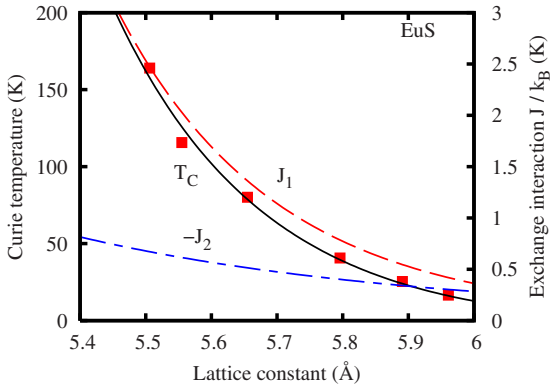

FIG. 8. (Color online) Critical temperatures and exchange interactions in EuS as a function of the lattice parameter. Squares correspond to measured Curie points in hydrostatic pressure experiments (Ref. 48); the solid line represents the least-square fit of Monte Carlo critical temperatures $T_C(J_1,J_2)$ based on the magnetic Grüneisen law $J_i(r_i) \sim r_i^{-n_i}$ with $n_1=22.4$ and $n_2=10$. The corresponding dependence of the nearest (J_1) and next-nearest-neighbor exchange interaction (J_2) on the lattice parameter is presented by the dashed and dashed-dotted line, respectively.

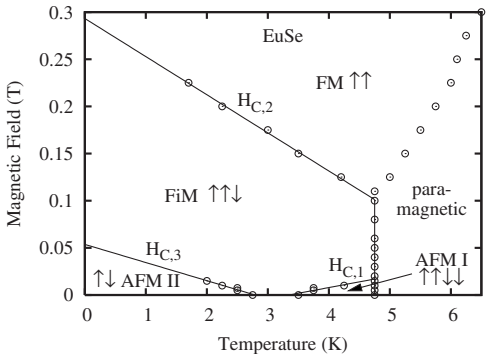

FIG. 9. Experimental magnetic phase diagram of unstrained EuSe. The phase boundaries (solid lines) are obtained from a linear least-square fit to experimental data (open symbols). See Ref. 11 for details.

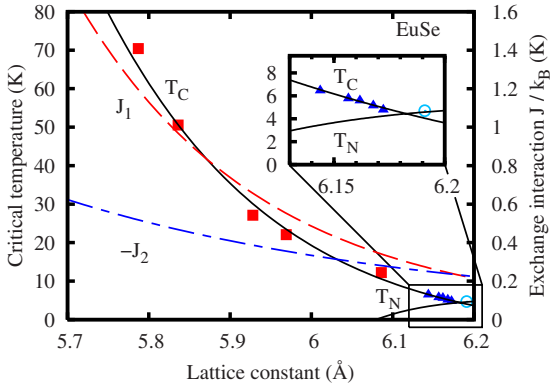

FIG. 10. (Color online) Critical temperatures and exchange interactions in EuSe as a function of lattice parameter. Filled symbols of triangles (Ref. 40) and squares (Ref. 48) correspond to measured Curie points in hydrostatic pressure experiments. The solid line (T_C) represents the least-square fit of the Monte Carlo $T_C(J_1, J_2)$ to the experimental Curie points based on the magnetic Grüneisen law $J_i(r_i) \sim r_i^{-n_i}$. The corresponding dependence of the nearest (J_1) and next-nearest-neighbor (J_2) exchange interaction as a function of lattice parameter is presented by the dashed and dashed-dotted lines, respectively. The inset shows the AFM I-FM transition occurring in EuSe at hydrostatic pressures around 0.5 GPa. The solid graph (T_N), which is based on an extrapolation of $J_1(a)$ and $J_2(a)$ toward a_0 corresponds to a theoretical AFM II Néel temperature, which is energetically comparable to the experimentally observed AFM I Néel point [open symbol (Refs. 11 and 40)].

turns out that because the NN exchange J_1 in EuO and EuS is always much larger than the NNN exchange J_2, the $T_C(a)$ dependence is quite insensitive to the variation in J_2 as a function of lattice constant, i.e., the fit yields only unreliable values for n_2. Because for EuTe we have already confirmed Bloch's 10/3 law for the volume dependence of the NNN superexchange integral J_2, we have therefore chosen to fix the distance dependence of $J_2(a)$ proportional to r_2^{-10} for EuO and EuS as well. From the fit, we then obtain $n_1^{\mathrm{EuO}} = 19.6 \pm 0.4$ and $n_1^{\mathrm{EuS}} = 22.4 \pm 0.3$ as the Grüneisen exponents for the NN exchange interaction $J_1(a)$. The resulting lattice-constant dependence of the Curie temperatures $T_C(a)$ and exchange interactions $J_1(a)$ and $J_2(a)$ are plotted in Fig. 7 for EuO and Fig. 8 for EuS as solid, dashed, and dashed-dotted lines, respectively. Evidently, an excellent fit with the experimental data is obtained over the whole lattice parameter range for both materials. This is an indication that the choice of $n_2 = 10$ is a reasonable assumption. It is also noted that due to the about a factor of 2 larger Grüneisen exponent of J_1 compared to that of J_2, at high hydrostatic pressures (small lattice constants), the NN exchange J_1 is as much as five times larger than the NNN exchange J_2. Thus, the ferromagnetic NN exchange completely dominates the magnetic behavior of both materials.

VI. EXCHANGE INTERACTION IN EuSe

Unlike EuO, EuS, and EuTe, which exhibit stable magnetic low-temperature phases, EuSe is a metamagnet with at least four different known ordered magnetic phases, i.e., two antiferromagnetic phases of type I (AFM I) and type II (AFM II), a FiM phase, and a FM phase. Figure 9 shows the *H-T* phase diagram of unstrained EuSe derived from susceptibility measurements on several micrometer thick epitaxial layers,[11] with the corresponding different spin configurations illustrated by the arrows. The phase boundaries shown in Fig. 9 are in good agreement with earlier publications.[9,10] In particular, the AFM I Néel point of $T_{N,\mathrm{AFM\ I}} = 4.7$ K and the critical field of $H_{C,3}(0) = 0.05$ T for the transition from AFM II to FiM obtained by linear extrapolation of the experimental AFM II to FiM phase boundary are in excellent agreement with those of Refs. 9 and 10.

The metamagnetic behavior of EuSe at ambient pressure shows similarities to the situation in EuTe at the AFM II to FM transition, occurring at a hydrostatic pressure of 9 GPa (see Fig. 3) where $J_1 \approx |J_2|$. The observation of an AFM I phase at this pressure that accompanies the AFM II to FM phase transition[46] shows that at this pressure EuTe is metamagnetic too. Thus, in both materials a metamagnetic behavior occurs when J_1 and $|J_2|$ are approximately equal and cancel each other. Then, otherwise negligible additional interactions come into play. As shown by Fig. 10, when applying a hydrostatic pressure above 0.5 GPa (Ref. 40) EuSe becomes a stable ferromagnet and with increasing pressure up to 15 GPa, i.e., 6% reduction in the lattice constant, the ferromagnetic ordering temperature T_C increases from 4.7 to above 70 K.[48] The corresponding experimental $T_C(a)$ data of EuSe is displayed as filled symbols in Fig. 10. Lechner *et al.*[11] also showed that the introduction of only little biaxial strain in EuSe drastically expands the boundaries of the AFM II phase and causes the AFM I phase to disappear completely. Thus, an AFM II to paramagnetic Néel point $T_{N,\mathrm{AFM\ II}}$ is observed in strained EuSe, which is again similar to the situation in EuTe.

The magnetic phase diagram of unstrained EuSe and its metastability for already small lattice deformations[11] cannot be described by isotropic NN and NNN Heisenberg exchange interactions alone. Especially, the ferrimagnetic and the AFM I phases, which show a magnetic structure with a periodicity of three, respectively, four atomic layers require further distant exchange interactions and/or other types of magnetic interactions such as long-range dipolar interactions.[10] Using MFA and a Hamiltonian, which in-

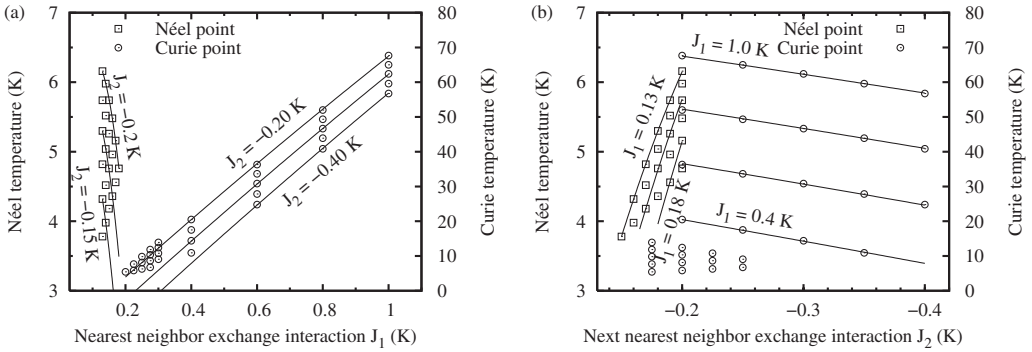

FIG. 11. Monte Carlo calculated critical temperatures of a bulk fcc Heisenberg system as a function of the strength of (a) the nearest and (b) next-nearest-neighbor exchange interactions J_1 and J_2, respectively, showing ferromagnetic to paramagnetic transitions if $J_1 > |J_2|$ and antiferromagnetic to paramagnetic transitions if $J_1 < |J_2|$. The parameter range corresponds to EuSe under hydrostatic pressures between 0 and around 15 GPa. Solid lines represent polynomial fit functions, which are quadratic in J_1 and J_2.

cludes the exchange interaction up to the third-nearest neighbor (J_3) and dipolar interactions, Fukuma *et al.*[10] showed that the critical field $H_{C,3}$ at $T=0$ is independent of J_3 and depends only on the sum (J_1+J_2) as well as the dipolar coupling strength D. Therefore, a good estimate of (J_1+J_2) can be obtained using the relation[10]

$$2(J_{1,0}+J_{2,0}) = -\frac{1}{3S}g\mu_B H_{C,3}(0) - \left[D_{xx}(\boldsymbol{Q_L}) - \frac{1}{9}D_{xx}(\mathbf{0}) - \frac{8}{9}D_{xx}\left(\frac{2}{3}\boldsymbol{Q_L}\right)\right], \tag{23}$$

where $D_{xx}(\boldsymbol{Q_L})$, $D_{xx}(\mathbf{0})$, and $D_{xx}(2\boldsymbol{Q_L}/3)$ correspond to the dipole coupling strength for spins lying in the (111) plane (see Ref. 10 for exact definitions). Inserting the measured $H_{C,3}(0)=0.05$ T and the calculated values of D_{xx} given in Ref. 10, we obtain $(J_1+J_2)/k_B=-5.2$ mK. Unlike for the other EuX compounds, we were not able to derive any further reliable condition that would allow to determine J_1 and J_2 independently of the high-pressure data in EuSe.

Since our Heisenberg spin model can only generate FM and AFM II orderings, we can only calculate the behavior of T_C as a function of lattice constant in the strain-induced ferromagnetic phase of EuSe at pressures above 0.5 GPa. In this region, third-nearest-neighbor exchange and dipolar interactions are not expected to contribute significantly to the ferromagnetic ordering. The corresponding ferromagnetic ordering temperatures calculated as a function of the NN and NNN Heisenberg exchange interactions in the range 0.2 K $\leq J_1/k_B \leq 1.0$ K and -0.175 K $\geq J_2/k_B \geq -0.4$ K with $J_1 > |J_2|$ are shown in Fig. 11. Evidently, $T_C(J_1,J_2)$ is slightly nonlinear in both J_1 and J_2 but approaches the relation given in Eq. (21) for $J_1 \gg -J_2$. We also simulated the AFM II to paramagnetic transitions for $J_1 < |J_2|$ in the interval 0.13 K $\leq J_1/k_B \leq 0.18$ K and -0.15 K $\geq J_2/k_B \geq -0.2$ K. The calculated critical temperature T_N as a function of the exchange constants J_1 and J_2 are shown in Figs. 11(a) and 11(b) as open squares. As in the case of EuTe, $T_N(J_1,J_2)$ is strongly nonlinear and both $T_C(J_1,J_2)$ and $T_N(J_1,J_2)$ were approximated by second-order polynomials as given in Eq. (19).

Inserting the magnetic Grüneisen law of Eq. (18) for $J_1(r_1)$ and $J_2(r_2)$ into the obtained $T_C(J_1,J_2)$ dependence, the distance dependence of the EuSe exchange constants $J_i(a)$ was again obtained by fitting the calculated $T_C(a)$ to the experimental Curie points of EuSe under hydrostatic pressure represented by the filled symbols. Other than in the preceding sections, not only the Grüneisen exponents n_1 and n_2 but also the ambient pressure exchange constants $J_{1,0}$ and $J_{2,0}$ were used as adjustable parameters in the fit routine, only restricted by the condition $(J_{1,0}+J_{2,0})/k_B=-5.2$ mK, as obtained from the critical field $H_{C,3}(0)$ as described above. Unlike the situation in EuO and EuS, the behavior of $J_2(a)$ influences the magnetic ordering considerably in the region close to a_0. Eventually, $J_{1,0}/k_B=0.223\pm0.016$ K, $J_{2,0}/k_B=-0.228\pm0.016$ K, $n_1=24.9\pm1.8$, and $n_2=12.2\pm6.0$ are obtained by the fit. As is demonstrated by the solid line in Fig. 10, with these parameters the experimental $T_C(a)$ data are precisely reproduced. The resulting dependence of J_1 and J_2 versus lattice constant are depicted as dashed, respectively, dashed-dotted lines in Fig. 10. At the bulk EuSe lattice constant of $a_0=6.191$ Å, the calculated J_2 is slightly larger in absolute value than J_1. This changes drastically as the lattice constant is reduced, with J_1 crossing J_2 already at low hydrostatic strain and J_1 becoming the dominant exchange interaction for $a<6.15$ Å. The Grüneisen exponents for the NN and the NNN exchange interactions are again in reasonable agreement with the results obtained for EuTe, EuO, and EuS.

To further justify our results on EuSe, we substituted the obtained $J_1(a)$ and $J_2(a)$ into the theoretical $T_N(J_1,J_2)$ AFM II to paramagnetic Néel function, obtained from the fit of Eq. (19) to the squares in Fig. 11. Extrapolating $T_N[J_1(a),J_2(a)]$ to the bulk lattice constant $a_0=6.191$ Å of EuSe, we obtained $T^{\mathrm{MC}}_{N,\mathrm{AFM\ II}}(a_0)=4.5$ K, which is, as expected, above the experimentally observed AFM II to FiM transition temperature of around 2 K (Refs. 9 and 11) but below the AFM I Néel point of 4.7 ± 0.1 K (Refs. 9, 11, and 40) (open symbol in Fig. 10). That the calculated AFM II to paramagnetic transition temperature of $T^{\mathrm{MC}}_{N,\mathrm{AFM\ II}}(a_0)$ is very close to the experimentally observed AFM I to paramagnetic $T_{N,\mathrm{AFM\ I}}$ is also expected in mean-field theory, where

$$T^{\mathrm{MFA}}_{N,\mathrm{AFM\ I}}(J_1,J_2) = 4S(S+1)J_1, \tag{24}$$

TABLE II. Distance dependence of nearest (subscript 1) and next-nearest-neighbor (subscript 2) exchange interactions of europium chalcogenides under hydrostatic pressure as obtained in our Monte Carlo study. For hydrostatic strains of typically less than ≈10%, the exchange interactions can equally well be described by either magnetic Grüneisen laws, $J_i = J_{i,0}(r_i/r_{0,i})^{-n_i}$ or by simple exponential laws, $J_i = J_{i,0}\exp[-\alpha_i(r_i - r_{0,i})]$—values labeled by *) are assumptions.

	EuTe	EuSe	EuS	EuO
a_0 (Å)	6.598	6.191	5.956	5.144
$T_N(a_0)$ (K)	9.85	4.7		
$T_C(a_0)$ (K)			16.6	69.15
$J_{1,0}/k_B$ (K)	0.192	0.223	0.427	1.169
n_1	20.6	24.9	22.4	19.6
α_1 (Å^{-1})	4.56	5.99	5.47	5.44
$J_{2,0}/k_B$ (K)	−0.313	−0.228	−0.306	−0.414
n_2	10.4	12.2	10*)	10*)
α_2 (Å^{-1})	1.63	2.31	1.68*)	1.94*)

$$T^{\mathrm{MFA}}_{N,\mathrm{AFM\ II}}(J_1,J_2) = -4S(S+1)J_2. \tag{25}$$

Thus, $T_{N,\mathrm{AFM\ I}}$ and $T_{N,\mathrm{AFM\ II}}$ are nearly equal when J_1 and J_2 are almost equal in strength. Moreover, it can easily be shown that taking third-nearest neighbor or biquadratic exchange terms into account would not favor either of the two antiferromagnetic ordering types (at least in the mean-field approximation) and the influence of dipolar interactions on the ordering temperatures is typically on the order of less than one Kelvin (see, e.g., Chap. 4 of Ref. 87). In addition, Lechner *et al.*'s (Ref. 11) results on biaxially strained EuSe indicate that the AFM I ordering observed in unstrained EuSe with $T_{N,\mathrm{AFM\ I}} \approx 4.7$ K is energetically only slightly lower than the Néel point $T_{N,\mathrm{AFM\ II}}$ of the AFM II ordering and a small biaxial strain already induces a transition from one to the other.

VII. DISCUSSION

The exchange constants of all four Eu*X* compounds and their dependence on the lattice parameter obtained by our MC analysis are summarized in Table II and Fig. 12. Evidently, in all cases, the bulk exchange constants $J_{1,0}$ and $J_{2,0}$ are almost a factor of 2 larger compared to the values reported in previous works, which in their analysis did not take spin fluctuations into account. More importantly, we have found that the magnetic properties and critical phase-transition temperatures of all Eu*X* compounds as a function of hydrostatic strain, i.e., lattice parameter can be consistently described by the magnetic Grüneisen power-law dependence $J_i(r_i) = J_{i,0}(r_i/r_{i,0})^{-n_i}$ with characteristic power-law exponents of $n_1 \approx 10$ for the NN exchange J_1 and of $n_2 \approx 20$ for the NNN exchange J_2 as indicated in Table II.

The corresponding dependence of the exchange interactions on the lattice constant $J_1(a)$ and $J_2(a)$ for all compounds is represented as dashed lines in Fig. 12. Evidently, neither $J_1(a)$ nor $J_2(a)$ are continuous functions over different members of the Eu*X* family. Therefore, the effect of the substitution of the anion elements cannot be simplified to a variation in the lattice constant alone, as was already noted in the previous work of Goncharenko *et al.*[54] In fact, as shown by Fig. 12, for a fixed lattice constant the absolute values of the exchange constants J_1 and J_2 are always much larger for the compound with larger anion element, i.e.,

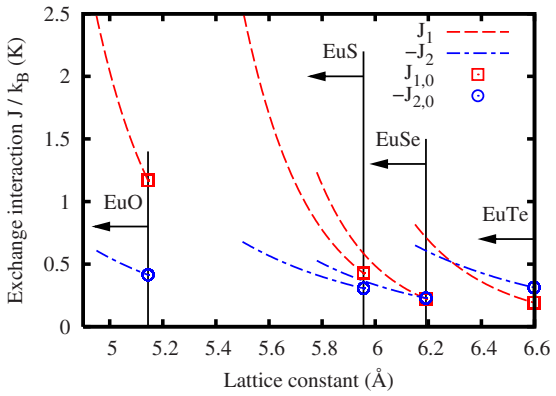

FIG. 12. (Color online) Summary of the exchange interactions in europium chalcogenides and their dependence on the lattice parameter as derived by Monte Carlo analysis.

$$|J_i^{\mathrm{EuTe}}(a)| \gg |J_i^{\mathrm{EuSe}}(a)| \gg |J_i^{\mathrm{EuS}}(a)| \gg |J_i^{\mathrm{EuO}}(a)|. \tag{26}$$

For this reason, at a given lattice parameter the ordering temperature is always significantly larger in EuTe compared to EuSe, EuS, and EuO. This is consistent with the extrapolation of the $T_C(a)$ data obtained from experiments.

Apart from the empirical magnetic Grüneisen law of Eq. (18) as the interatomic distance dependence of the exchange interactions in the Eu*X*'s, we have also explored, whether different functional dependencies might reproduce the experimental ordering temperatures as functions of the lattice constant as well. Due to the strong superlinear increase in the ferromagnetic ordering temperature with decreasing lattice constant and the fact that $T_C(J_1,J_2)$ behaves very close to linear in all Eu*X* compounds, a linear distance dependence of the exchange interactions can be categorically ruled out. One other empirical form of $J(r)$, which could be expected from the nature of quantum-mechanical two-electron multicenter integrals, e.g., the Heitler-London approach to solve the Schrödinger equation for the hydrogen molecule,[88] is a simple exponential distance law of the form

$$J(r) = J_0 \exp[-\alpha(r - r_0)], \tag{27}$$

$$= J_0 \exp[-\alpha r_0(r/r_0 - 1)], \tag{28}$$

where $J(r_0) = J_0$ is again the exchange constant under normal condition. Applying this exponential law in the simulated critical temperatures $T_N(J_1,J_2)$ and $T_C(J_1,J_2)$ and fitting the experimental critical points of the Eu*X*'s as functions of the lattice constant, it turns out, that the results for $J_1(a)$ and $J_2(a)$ are practically indistinguishable from those received by employing the Grüneisen power law. In essence, the calculated $T_N(a)$ and $T_C(a)$ curves as well as the $J_1(a)$ and $J_2(a)$ distance dependencies of the exchange interactions coincide

almost exactly with those depicted in Fig. 12. The reason for this unambiguity is that the variations in the interatomic distances achievable by hydrostatic pressure experiments are too small ($\leq 8\%$) to be able to definitely single out between the two functional dependencies. However, while the distance dependence of the exchange interactions for the different members of the EuX family show consistent and universal Grüneisen exponents n_i for the NN as well as the NNN exchange interactions, such a similarity cannot be found for the scaling factors α_i in the simple exponential description. This is illustrated by Table II, where the α_i, n_i, and $J_{0,i}$ of all EuX compounds derived in this work are listed, showing that α_1 varies in the range of 4.5–6 Å^{-1} and α_2 from 1.6–2.3 Å^{-1}. This difference follows from the fact that only the magnetic Grüneisen law of Eq. (18) is defined in terms of relative changes in the lattice parameter r/r_0. For a better comparison, the exponential distance law of Eq. (27) must be therefore rewritten as a function of r/r_0 as represented by Eq. (28). Then αr_0 represents a dimensionless scaling factor that can be compared for the different members of the EuX family. As it turns out, the values for $\alpha_i r_0$ are approximately equal to the respective n_i's for all EuX compounds. This observation becomes clear from a mathematical point of view because the relation[89]

$$\alpha = -\frac{\frac{dJ}{dr}(r)}{J(r)} \tag{29}$$

and the requirement that both $J(r)$ and its derivative with respect to r have to match at r_0 yields the relation $n=\alpha r_0$. Thus, for small deviations of r from r_0 the power law and the exponential dependence are practically equivalent when α is chosen as $\alpha=n/r_0$.

The theoretical derivation of analytic scaling laws for the distance dependence of the exchange interactions is far from trivial and estimates can only be obtained as far as the exchange mechanisms are understood. According to Kasuya[4] the most important contribution to the NN exchange interaction consists of a virtual excitation of a Eu^{2+} $4f$ electron to the $5d$ state of a NN cation and a subsequent intra-atomic d-f exchange. For this type of exchange, a distance dependence $J_1(r_1) \sim \exp(-8r_1/r_0)$ is considered. The NNN exchange may consist of several competing components, which are considered to involve excitations of the anion p electrons to neighboring cation $5d$ states. Kasuya did not give an estimate for the distance dependence of the NNN superexchange. Lee and Liu,[71] on the other hand, proposed interband exchange mechanisms for both J_1 and J_2 where the exchange of the localized $4f$ moments is mediated by virtual excitations of chalcogenide-valence-band p electrons into the empty Eu^{2+} $5d$ conduction bands, together with a subsequent interband exchange of the d electron (p hole) with the localized $4f$ electrons. In this semiconductor analog of the Ruderman-Kittel-Kasuya-Yosida interaction $J(r) \sim r^{-4}$ is considered for the distance dependencies of the NN and NNN exchange interactions. Both estimates for the distance dependence of the exchange interactions more or less support the picture[1–3,90] of the exchange interactions being continuous functions across different members of the EuX family. Our analysis clearly shows that the exchange interactions vary much stronger as a function of the interatomic distances than previously assumed. With a Grüneisen exponent of $n_1 \approx 20$, there is a particularly strong dependence of the NN exchange J_1 on the interatomic distances and the exponent $n_2 \approx 10$ for the NNN interaction J_2 agrees exactly with Bloch's (Ref. 57) empirical 10/3 law for the volume dependence of the superexchange in magnetic solids. The conclusion from Fig. 12 that the differences in the magnetic ordering temperatures between the EuX compounds cannot be attributed solely to the differences in the lattice parameters is supported by recent spectroscopic x-ray absorption experiments and *ab initio* calculations by Souza-Neto *et al.*[91] that showed that the substitution of the anion elements not only changes the magnitude of Eu f-d intermixing but also affects the f-d-p hybridization via the anion p states. This partially counteracts the increase in the ordering temperatures otherwise expected from the decrease in lattice constant when going from EuTe to EuO.

The possibility to integrate EuO with Si and GaN (Refs. 31 and 32) together with the fact that T_C can be increased by doping[33,34] and hydrostatic strain[44,45,92] to temperatures up to 200 K led to a renewed interest in the ferromagnetic europium monochalcogenides as possible materials for spintronic devices. As hydrostatic pressure is not an option for practical applications, epitaxial strain has been suggested as an alternative way to increase the ferromagnetic ordering temperature in EuO.[93] Ingle and Elfimov showed in their *ab initio* study that biaxial compressive strain increases T_C in EuO similarly to the situation in EuSe (Ref. 11) and EuTe,[52,53] where the antiferromagnetic ordering temperature was shown to increase with reduction in in-plane lattice constant of strained epilayers. This increase can be easily reproduced by Monte Carlo calculations with proper adjustment of the exchange constants and in this way the magnetic behavior even of ultrathin EuTe layers can be precisely described.[53]

VIII. CONCLUSION

In summary, we have applied the Monte Carlo method to determine the exchange integrals in the EuX compounds. To this end, we have determined the general dependences of the magnetic ordering temperatures, i.e., ferromagnetic $T_C(J_1,J_2)$ and antiferromagnetic $T_N(J_1,J_2)$ as a function of the NN and NNN exchange interactions of a system of classical Heisenberg spins at the sites of an fcc lattice. This was subsequently applied to determine the dependence of the NN and NNN exchange interactions J_1 and J_1 on the interatomic distances r_i between the Eu ions from hydrostatic pressure experiments using the magnetic Grüneisen law[57] $J_i(r_i) \sim r_i^{-n_i}$. For all members of the EuX family, the experimental data can be consistently described by universal Grüneisen exponents $n_1 \approx 20$ and $n_2 \approx 10$. The latter conforms exactly with

Bloch's empirical 10/3 law for the volume dependence of the superexchange interaction.[57] Although an exponential distance dependence can also be fitted to the experimental data, no universal scaling behavior is found in this case. Comparing the different EuX compounds, it is also found that the interaction constants change discontinuously when the anion elements change from X=Te, Se, S, to O because the different anion electron affinity changes the hybridization and mixing of the electronic bands responsible for the coupling of the magnetic moments. Thus, the differences in the exchange constants cannot be merely attributed to the difference in the lattice constants in this case. On the other hand, the strong increase in the exchange constants with decreasing lattice parameter provides ample room for increasing the magnetic ordering temperatures in strained heteroepitaxial structures, which is an important prerequisite for device applications.

ACKNOWLEDGMENTS

This work was supported by the Austrian Science Funds FWF, the FONE-Program of the ESF (SPINTRA), the Gesellschaft fuer Mikro- and Nanoelektronik, Vienna, and the Austrian NANO Initiative (NSI). The authors would like to thank Reinhard Folk for useful hints and valuable discussions and Daniel Gruber and Johann Messner for technical assistance.

*Author to whom correspondence should be addressed; gunther.springholz@jku.at

[1] W. Zinn, J. Magn. Magn. Mater. **3**, 23 (1976).
[2] P. Wachter, in *Handbook on the Physics and Chemistry of the Rare Earths*, edited by K. A. Gschneidner, Jr. and L. Eyring (Elsevier, North-Holland, Amsterdam, 1979), Vol. 2, p. 507.
[3] A. Mauger and C. Godart, Phys. Rep. **141**, 51 (1986).
[4] T. Kasuya, IBM J. Res. Dev. **14**, 214 (1970).
[5] M. S. Seehra and T. M. Giebultowicz, Phys. Rev. B **38**, 11898 (1988).
[6] B. T. Matthias, R. M. Bozorth, and J. H. Van Vleck, Phys. Rev. Lett. **7**, 160 (1961).
[7] T. R. McGuire, B. E. Argyle, M. W. Shafer, and J. S. Smart, Appl. Phys. Lett. **1**, 17 (1962).
[8] N. F. Oliveira, Jr., S. Foner, Y. Shapira, and T. B. Reed, Phys. Rev. B **5**, 2634 (1972).
[9] R. Griessen, M. Landolt, and H. R. Ott, Solid State Commun. **9**, 2219 (1971).
[10] H. Fukuma, T. Komatsubara, T. Suzuki, E. Kaldis, and T. Kasuya, J. Phys. Soc. Jpn. **54**, 3067 (1985).
[11] R. T. Lechner, G. Springholz, T. U. Schülli, J. Stangl, T. Schwarzl, and G. Bauer, Phys. Rev. Lett. **94**, 157201 (2005).
[12] R. Kirchschlager, W. Heiss, R. T. Lechner, G. Bauer, and G. Springholz, Appl. Phys. Lett. **85**, 67 (2004).
[13] W. Heiss, G. Prechtl, and G. Springholz, Phys. Rev. B **63**, 165323 (2001).
[14] P. G. Steeneken, L. H. Tjeng, I. Elfimov, G. A. Sawatzky, G. Ghiringhelli, N. B. Brookes, and D.-J. Huang, Phys. Rev. Lett. **88**, 047201 (2002).
[15] T. S. Santos and J. S. Moodera, Phys. Rev. B **69**, 241203(R) (2004).
[16] T. S. Santos, J. S. Moodera, K. V. Raman, E. Negusse, J. Holroyd, J. Dvorak, M. Liberati, Y. U. Idzerda, and E. Arenholz, Phys. Rev. Lett. **101**, 147201 (2008).
[17] J. S. Moodera, X. Hao, G. A. Gibson, and R. Meservey, Phys. Rev. Lett. **61**, 637 (1988).
[18] X. Hao, J. S. Moodera, and R. Meservey, Phys. Rev. B **42**, 8235 (1990).
[19] A. T. Filip, P. LeClair, C. J. P. Smits, J. T. Kohlhepp, H. J. M. Swagten, B. Koopmans, and W. J. M. de Jonge, Appl. Phys. Lett. **81**, 1815 (2002).
[20] P. LeClair, J. K. Ha, H. J. M. Swagten, J. T. Kohlhepp, C. H. van de Vin, and W. J. M. de Jonge, Appl. Phys. Lett. **80**, 625 (2002).
[21] C. J. P. Smits, A. T. Filip, J. T. Kohlhepp, H. J. M. Swagten, B. Koopmans, and W. J. M. de Jonge, J. Appl. Phys. **95**, 7405 (2004).
[22] J. Trbovic, C. Ren, P. Xiong, and S. von Molnár, Appl. Phys. Lett. **87**, 082101 (2005).
[23] T. Nagahama, T. S. Santos, and J. S. Moodera, Phys. Rev. Lett. **99**, 016602 (2007).
[24] C. Ren, J. Trbovic, R. L. Kallaher, J. G. Braden, J. S. Parker, S. von Molnár, and P. Xiong, Phys. Rev. B **75**, 205208 (2007).
[25] J. S. Moodera, R. Meservey, and X. Hao, Phys. Rev. Lett. **70**, 853 (1993).
[26] G. Busch, J. Schoenes, and P. Wachter, Solid State Commun. **8**, 1841 (1970).
[27] J. Schoenes and P. Wachter, Physica B & C **86-88**, 125 (1977).
[28] M. Suekane, G. Kido, N. Miura, and S. Chikazumi, J. Magn. Magn. Mater. **31-34**, 589 (1983).
[29] H. Hori, R. Akimoto, M. Kobayashi, S. Miyamoto, M. Furusawa, N. Kreines, A. Yamagishi, and M. Date, Physica B **201**, 438 (1994).
[30] M. R. Koblischka and R. J. Wijngaarden, Supercond. Sci. Technol. **8**, 199 (1995).
[31] J. Lettieri, V. Vaithyanathan, S. K. Eah, J. Stephens, V. Sih, D. D. Awschalom, J. Levy, and D. G. Schlom, Appl. Phys. Lett. **83**, 975 (2003).
[32] A. Schmehl *et al.*, Nature Mater. **6**, 882 (2007).
[33] T. J. Konno, N. Ogawa, K. Wakoh, K. Sumiyama, and K. Suzuki, Jpn. J. Appl. Phys. **35**, 6052 (1996).
[34] H. Ott, S. J. Heise, R. Sutarto, Z. Hu, C. F. Chang, H. H. Hsieh, H.-J. Lin, C. T. Chen, and L. H. Tjeng, Phys. Rev. B **73**, 094407 (2006).
[35] D. B. McWhan, P. C. Souers, and G. Jura, Phys. Rev. **143**, 385 (1966).
[36] V. C. Srivastava and R. Stevenson, Can. J. Phys. **46**, 2703 (1968).
[37] U. F. Klein, G. Wortmann, and G. M. Kalvius, J. Magn. Magn. Mater. **3**, 50 (1976).
[38] U. F. Klein, J. Moser, G. Wortmann, and G. M. Kalvius, Physica B **86-88**, 118 (1977).
[39] J. Moser, G. Wortmann, N. Bykovetz, and G. M. Kalvius, J.

Magn. Magn. Mater. **12**, 77 (1979).
[40] H. Fujiwara, H. Kadomatsu, M. Kurisu, T. Hihara, K. Kojima, and T. Kamigaichi, Solid State Commun. **42**, 509 (1982).
[41] C. Sauer, A. Zaker, and W. Zinn, J. Magn. Magn. Mater. **31-34**, 423 (1983).
[42] T. Hihara, K. Hiraoka, K. Kojima, T. Kamigaichi, and T. Kino, J. Magn. Magn. Mater. **52**, 443 (1985).
[43] V. G. Tissen and E. G. Ponyatovskii, JETP Lett. **46**, 361 (1987).
[44] J. Moser, G. M. Kalvius, and W. Zinn, Hyperfine Interact. **41**, 499 (1988).
[45] M. M. Abd-Elmeguid and R. D. Taylor, Phys. Rev. B **42**, 1048 (1990).
[46] I. N. Goncharenko and I. Mirebeau, Europhys. Lett. **37**, 633 (1997).
[47] M. Ishizuka, Y. Kai, R. Akimoto, M. Kobayashi, K. Amaya, and S. Endo, J. Magn. Magn. Mater. **166**, 211 (1997).
[48] I. N. Goncharenko and I. Mirebeau, Phys. Rev. Lett. **80**, 1082 (1998).
[49] G. Springholz and G. Bauer, Phys. Rev. B **48**, 10998 (1993).
[50] N. Frank, G. Springholz, and G. Bauer, Phys. Rev. Lett. **73**, 2236 (1994).
[51] A. Stachow-Wójcik *et al.*, Phys. Rev. B **60**, 15220 (1999).
[52] H. Kępa, G. Springholz, T. M. Giebultowicz, K. I. Goldman, C. F. Majkrzak, P. Kacman, J. Blinowski, S. Holl, H. Krenn, and G. Bauer, Phys. Rev. B **68**, 024419 (2003).
[53] E. Schierle, E. Weschke, A. Gottberg, W. Söllinger, W. Heiss, G. Springholz, and G. Kaindl, Phys. Rev. Lett. **101**, 267202 (2008).
[54] I. N. Goncharenko, I. Mirebeau, and A. Ochiai, Hyperfine Interact. **128**, 225 (2000).
[55] D. P. Landau and K. Binder, *A Guide to Monte Carlo Simulations in Statistical Physics* (Cambridge University Press, Cambridge, England, 2000).
[56] S. M. Scott and T. M. Giebultowicz, J. Appl. Phys. **91**, 8724 (2002).
[57] D. Bloch, J. Phys. Chem. Solids **27**, 881 (1966).
[58] G. Springholz and G. Bauer, Appl. Phys. Lett. **62**, 2399 (1993).
[59] N. Metropolis, A. W. Rosenbluth, M. N. Rosenbluth, A. H. Teller, and E. Teller, J. Chem. Phys. **21**, 1087 (1953).
[60] D. S. Ritchie and M. E. Fisher, Phys. Rev. B **5**, 2668 (1972).
[61] P. Peczak, A. M. Ferrenberg, and D. P. Landau, Phys. Rev. B **43**, 6087 (1991).
[62] K. Chen, A. M. Ferrenberg, and D. P. Landau, Phys. Rev. B **48**, 3249 (1993).
[63] R. M. Nowotny and K. Binder, Z. Phys. B: Condens. Matter **77**, 287 (1989).
[64] W. Nolting, *Quantentheorie des Magnetismus* (B. G. Teubner, Stuttgart, 1986), Vol. 2.
[65] P. W. Anderson, Phys. Rev. **83**, 1260 (1951).
[66] W. Heiss, G. Prechtl, and G. Springholz, Appl. Phys. Lett. **78**, 3484 (2001).
[67] W. Heiss, R. Kirchschlager, G. Springholz, Z. Chen, M. Debnath, and Y. Oka, Phys. Rev. B **70**, 035209 (2004).
[68] M. E. Fisher, Philos. Mag. **7**, 1731 (1962).
[69] U. Köbler, I. Apfelstedt, K. Fischer, W. Zinn, E. Scheer, J. Wosnitza, H. v. Löhneysen, and T. Brückel, Z. Phys. B: Condens. Matter **92**, 475 (1993).
[70] J. Kunes, W. Ku, and W. E. Picket, J. Phys. Soc. Jpn. **74**, 1408 (2005).
[71] V.-C. Lee and L. Liu, Phys. Rev. B **30**, 2026 (1984).
[72] D. I. Khomskii and G. A. Sawatzky, Solid State Commun. **102**, 87 (1997).
[73] A. Radomska and T. Balcerzak, Phys. Status Solidi B **225**, 229 (2001).
[74] L. Passell, O. W. Dietrich, and J. Als-Nielsen, Phys. Rev. B **14**, 4897 (1976).
[75] H. G. Bohn, W. Zinn, B. Dorner, and A. Kollmar, J. Appl. Phys. **52**, 2228 (1981).
[76] H. A. Mook, Phys. Rev. Lett. **46**, 508 (1981).
[77] B. C. Passenheim, D. C. McCollum, Jr., and J. Callaway, Phys. Lett. **23**, 634 (1966).
[78] J. A. J. Henderson, G. R. Brown, T. B. Reed, and H. Meyer, J. Appl. Phys. **41**, 946 (1970).
[79] P. K. Schwob and G. E. Everett, J. Phys. Colloq. (Paris) **32**, C1-1066 (1971).
[80] O. W. Dietrich, A. J. Henderson, and H. Meyer, Phys. Rev. B **12**, 2844 (1975).
[81] S. H. Charap and E. L. Boyd, Phys. Rev. **133**, A811 (1964).
[82] E. L. Boyd, Phys. Rev. **145**, 174 (1966).
[83] A. Comment, J.-P. Ansermet, C. P. Slichter, H. Rho, C. S. Snow, and S. L. Cooper, Phys. Rev. B **72**, 014428 (2005).
[84] P. K. Schwob, M. Tachiki, and G. E. Everett, Phys. Rev. B **10**, 165 (1974).
[85] S. Heathman, T. Le Bihan, S. Darracq, C. Abraham, D. J. A. De Ridder, U. Benedict, K. Mattenberger, and O. Vogt, J. Alloys Compd. **230**, 89 (1995).
[86] H. G. Zimmer, K. Takemura, K. Syassen, and K. Fischer, Phys. Rev. B **29**, 2350 (1984).
[87] S. Blundell, *Magnetism in Condensed Matter*, Oxford Master Series in Condensed Matter Physics (Oxford University Press, New York, 2001).
[88] W. Heitler and F. London, Z. Phys. A **44**, 455 (1927).
[89] R. E. Coffman and G. R. Buettner, J. Phys. Chem. **83**, 2387 (1979).
[90] T. R. McGuire and M. W. Shafer, J. Appl. Phys. **35**, 984 (1964).
[91] N. M. Souza-Neto, D. Haskel, Y.-C. Tseng, and G. Lapertot, Phys. Rev. Lett. **102**, 057206 (2009).
[92] D. DiMarzio, M. Croft, N. Sakai, and M. W. Shafer, Phys. Rev. B **35**, 8891 (1987).
[93] N. J. C. Ingle and I. S. Elfimov, Phys. Rev. B **77**, 121202(R) (2008).